ADVANCED FUNCTIONAL MATERIALS
www.afm-journal.de

A Facile In Situ Approach to Polypyrrole Functionalization Through Bioinspired Catechols

*Wei Zhang, Zihe Pan, Fut K. Yang, and Boxin Zhao**

A template-free benign approach to modify polypyrrole (PPy) with bioinspired catechol derivatives dopamine (DA), 1,2-dihydroxybenzene or catechol (CA), and L-3,4-dihydroxyphenylalanine (DOPA) is reported. It is found that PPy functionalized with these catechol derivatives (DA, CA, and DOPA) exhibited fibrous structure, smaller particle size, good water dispersibility, and enhanced film adhesion. Surprisingly, it is found that adding a small amount of catechols can also improve PPy's electrical conductivity. This rapid, one-step, in situ, template-free method provided an alternative strategy to the facile production of PPy fibers. Among these three catechols, functionalized PPy and DA-PPy exhibits the smallest particle size and best performance in both adhesion and electrical conductivity. In contrast, the control phenylethlamine (PA) modification had almost negligible influence on the PPy properties, which provides strong evidence that instead of amine functional group or coexistence of both catechol and amine moieties, catechol itself is responsible for the successful functionalization of PPy and overall performance improvement. Furthermore, catechol-PPy nanofibers are blended into polyvinyl alcohol (PVA) aqueous solution and casted to form thin films; as-synthesized conductive films are found able to bond strongly onto the surface and may find broad applications in manufacturing biosensors and electronic devices.

1. Introduction

The catechol derivatives, which contain a distinct structure of a benzene ring with two neighboring hydroxyl groups, are found ubiquitously in nature. They exist in a variety of living systems and participate in a broad range of biochemical processes.[1] For example, catecholamines including epinephrine, noradrenaline, and dopamine (DA) are biologically significant hormones and neurotransmitters that are responsible for conveying nerve impulses, regulating heart rate, and controlling the brain's oxygen supply in the human body.[2] Marine mussels secrete L-3,4-dihydroxyphenylalanine (DOPA) containing adhesive proteins to adhere on different surfaces under wet conditions.[3] Catechol-based materials are commonly prepared by self-assembly of catechol functional groups induced by alkaline pH, enzymatic oxidation or electropolymerization. More recently, Ruiz-Molina developed a novel strategy where catechol-based materials can be obtained by the polymerization of functionalized catechols with ammonia, significantly broadening the potential applications of such materials.[4] Catechol moieties are remarkably reactive, they can undergo many types of chemical reactions, which are summarized in **Figure 1**.[5] The presence of the hydroxyl groups at the *ortho*-position makes this moiety ideal for chelating many di- or tri-valent metal ions to form stable complexes. Also, they can strongly interact with various organic materials through covalent bonding, π–π stacking, and hydrogen bonding.[6] Moreover, catechols can be oxidized into semiquinone radicals and *o*-benzoquinones, which are sensitive to both thiols and nitrogen derivatives, such as proteins and amino acid, to form thiol adduct, amine adduct or *o*-quinonimine via Schiff base formation and Michael-type addition under basic conditions.[5] Due to such versatility, catechol-based materials have been subjected to intense investigations, leading to the design and development of a large number of applications in biomedical engineering, nanotechnology, and material science.[7]

The excellent adhesion is one of the most astonishing properties offered by catechol compounds.[8] With regard to this functional role, great efforts have been devoted towards exploiting catechols for the modification of synthetic materials with enhanced interfacial adhesion.[9] The general strategy of formulating adherent materials is that catechol moieties can either be directly incorporated into the polymer backbone, or be grafted onto macromolecules as side and end-chain groups. Lee et al. prepared a series of linear and branched poly(ethylene glycol) hydrogels modified with 1–4 catechol end groups, which exhibited enhanced mucoadhesivity and can be used for medical applications.[10] Westwood et al. distributed catechol functionalities into polystyrene backbone to form a class of block copolymers with improved adhesive strength.[11] On the contrary, catechols can act as cross-linkers to constitute the framework of 2D or 3D architectures, either by selfpolymerization or coordination to metal irons. In particular, catechol functionalized cellulose nanofibers displayed much stronger adhesive forces to inorganic surfaces in the presence of Fe^{3+} ions, which

W. Zhang, Z. Pan, F. K. Yang, Prof. B. Zhao
Department of Chemical Engineering
Waterloo Institute for Nanotechnology
University of Waterloo
200 University Avenue West
Waterloo, Ontario, N2L 3G1, Canada
E-mail: zhaob@uwaterloo.ca

DOI: 10.1002/adfm.201403115

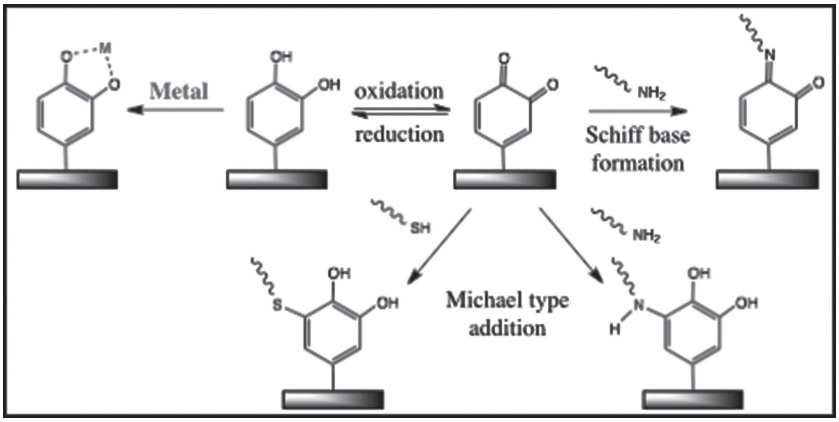

Figure 1. Possible chemical reactive pathways of catechol functional group.

can be attributed to the bridging force provided by the formation of the Fe(catechol)$_3$ complex.[12]

In addition to being used as a universal platform for developing adherent complexes, catechol moieties have also emerged as multifunctional coating materials for the surface modification of various substrates.[13] Inspired by the mussel adhesive proteins, a simple catechol derivative, DA has been found able to oxidize and self-polymerize to form a nanoscale polydopamine (PDA) film on virtually all surfaces in basic conditions.[14] Notwithstanding that the DA polymerization mechanism is still not clear,[15] PDA has arisen as a promising research subject in various fields ranging from the fabrication of energetic coatings to the preparation of functional composite materials.[16,17] We have a standing interest in PDA chemistry, and we have applied PDA to the syntheses of functional nanocomposites.[18–20] We reported some preliminary results of using dopamine to modify electrically conductive polypyrrole (PPy), which resulted in the improved dispersion in water and film adhesion in a recent communication paper.[20]

PPy displays many striking properties, such as facile synthesis, long-term stability, high conductivity, and good biocompatiablity.[21] However, this unique conducting polymer bears its own down-side: PPy forms large particles that precipitate in water and in most of organic solvents, as well as its poor mechanical and adhesion properties, making it difficult to process and functionalize for practical engineering.[22,23] In the previous studies, we employed in situ polymerization of pyrrole (Py) with DA, and discovered that after being functionalized by DA, the morphology of PPy changed from globular to fibrous; the adhesion between PPy film and glass substrates was enhanced. In this paper, we report a detailed and systematic investigation using three types of bioinspired catechol derivatives (simple catechol (CA) and DOPA in addition to the dopamine) and 2-phenylethylamine (PA) in the synthesis of PPy. These studies have provided strong evidence that catechol modification can be applied as a general protocol to functionalize conducting polymers to overcome the problem of poor water dispersibility and low interfacial adhesion of PPy. As a result of improved adhesion and dispersion, we demonstrated that modified PPy can be uniformly dispersed into polyvinyl alcohol (PVA) polymer matrix and casted to form thin films, which have been found able to maintain mechanical integrity at much higher load and stress level compared with DA-PPy films casted in water. The capability of resisting mechanical strains and stresses, combined with high conductivity, as-fabricated DA-PPy/PAV coating could find broad applications in electronic device manufacturing.

2. Results and Discussion

2.1. Morphological and Structural Characteristics of Functionalized PPy

To investigate the effect of different functional groups (dicatechol and amine) on the morphologies of the resulting PPy nanostructures, pyrrole (Py) was polymerized at the presence of DA, CA, DOPA, and PA, respectively. All of the experiments were carried out under the same reaction conditions so as to compare the modified PPy powder structures, which were characterized by scanning electron microscope (SEM) and showed in **Figure 2**. From Figure 2a–c, we found that catechol derivatives (DA, CA, and DOPA) modified PPy-exhibited fibrous morphology, while PA modified PPy presented globular shape, with a diameter of about 250 nm (Figure 2d), which is almost identical to the pure PPy nanostructure.[20] The PPy fibers obtained by reacting with catechol derivatives were twisted and tangled, and their aggregates are compact due to the strong hydrogen bonding and π–π interactions. Each individual fiber was further analyzed by transmission electron microscopy (TEM) as

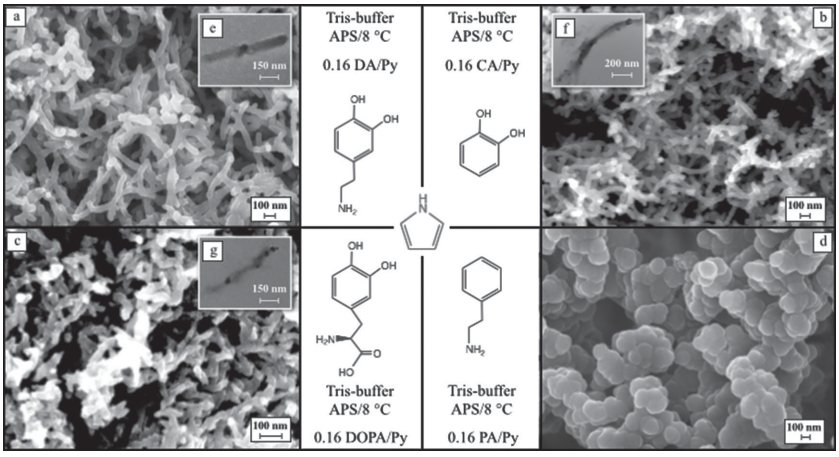

Figure 2. SEM images of a) fibrous DA-PPy morphology; b) fibrous CA-PPy morphology; c) fibrous DOPA-PPy morphology; and d) PA-PPy with globular shape. TEM topography images of a single fiber resulted from e) 0.16 DA/Py reacting mole ratio; f) 0.16 CA/Py reacting mole ratio; and g) 0.16 DOPA/Py reacting mole ratio.

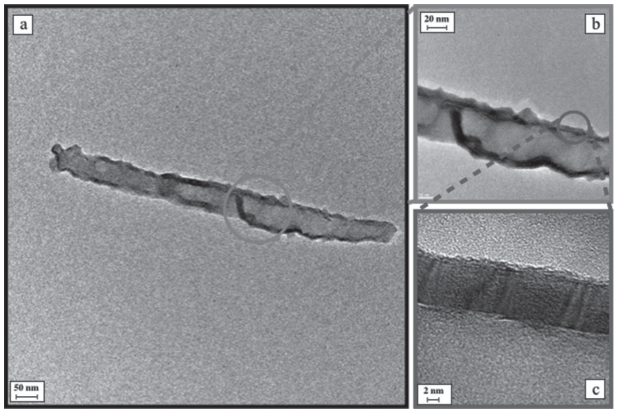

Figure 3. a) TEM topography image of a single DA-PPy fiber resulted from 0.64 DA/Py reacting mole ratio; b) the core/shell structure of the PDA-PPy fiber; and c) a detailed image of the PDA coating.

shown in Figure 2e–g; it was found that these nanofibers had a diameter ranging from 40 to 70 nm, and a length up to 1 μm. The TEM image (**Figure 3**a) shows a single DA-PPy fiber morphology resulted from the 0.64 DA/Py reacting mole ratio. A detailed image (Figure 3b) reveals a core/shell structure of the fiber, and its coating shell is shown in Figure 3c. These images suggest that there is possible phase segregation between the PPy and the catechol phase. The fabrication of fibrillar PPy has already been demonstrated by previous works since controlling the morphology and shape is a key criterion when integrating PPy into microelectronic devices.[24] For example, Martin et al. prepared PPy tubes against anodic aluminum oxide (AAO) template;[25] Manohar et al. reported the syntheses of PPy nanotubes with narrow pore size (10 nm) by using V_2O_5 nanofibers template;[26] Wu et al. employed MnO_2 nanowires as a reactive template to yield PPy fiber.[27] However, these approaches all suffer from using complicated procedures to remove the sacrificial templates. Our approach is rapid, one-step, in situ, and template-free; it provides an alternative strategy to the facile production of PPy nanofibers.

Since there is no template to guide the Py growth, we attributed the formation of catechol-PPy fibrous structures to the following phenomena and facts as we observed in our own experiments and reported in recent literature. Firstly, as revealed in Figure 2, the fibrillar morphology of catechol-PPy can only be constructed by in situ polymerization of Py in the presence of catechol derivatives. We believe those catechol-PPy fibers must contain catechol derivatives. Secondly, during the polymerization process, di-catechol functional group can be oxidized to *o*-quinonimine, which can chemically react with Py ring to minimize the formation of interchain links and side chains in the PPy network. **Figure 4**a illustrated the chemical structures of possible interchain links (connecting the nearest two PPy backbones) and side chains (connecting to one PPy backbone) through 2,3/3,3 coupling of the Py.[28] Although most of the PPy chains are straight and Py rings are linked at the 2,5 positions, Pfluger and co-workers found that 33% of the Py rings were affected by structural disorder (cross-linked or chain-terminating) based on X-ray photoelectron spectroscopy (XPS) studies.[29] Thus, by reacting with *o*-quinonimine functional group, β-sites of the Py can be blocked to ensure a completely α–α bonded linear chain propagation, which exhibits an ordered fibrous structure. Due to the universal driving force by surface energy minimization, the hydrophobic polymer long chains tend to entangle and twist in water; in the case of pristine PPy, this phenomenon may be more pronounced because of the strong hydrogen bonding and π–π interactions between each Py unit as illustrated in Figure 4b. Therefore, pristine PPy exhibits granular morphology. However, after incorporating catechol derivatives, PPy polymer chains became shorter, more hydrophilic, and more sterically hindered. All of these changes may effectively prevent the agglomeration and entanglement of PPy chain, resulting in fibrous morphology of catechol-PPy.

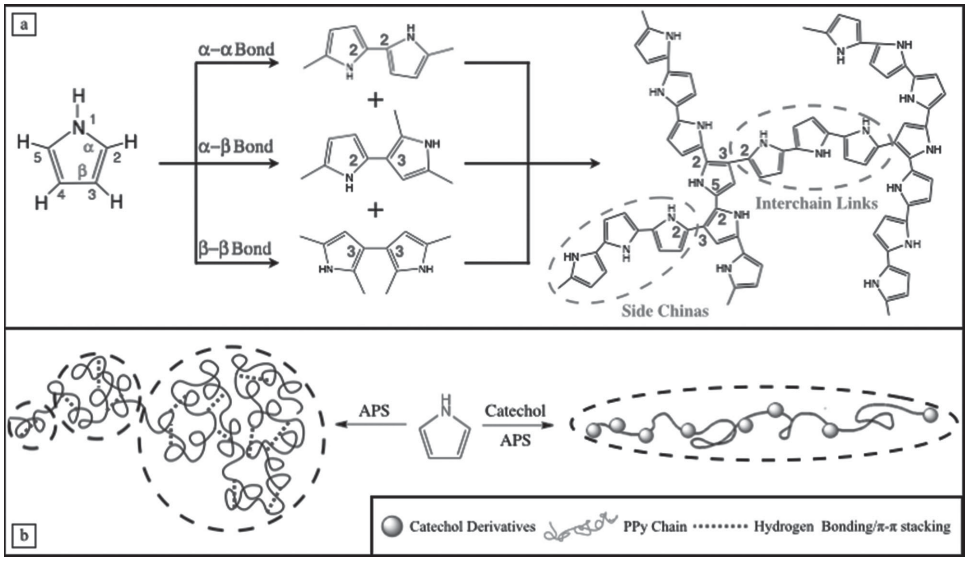

Figure 4. a) Chemical structures of interchain links and side chains, and their formation mechanism; b) a schematic illustration PPy globular and fibrous morphology formation.

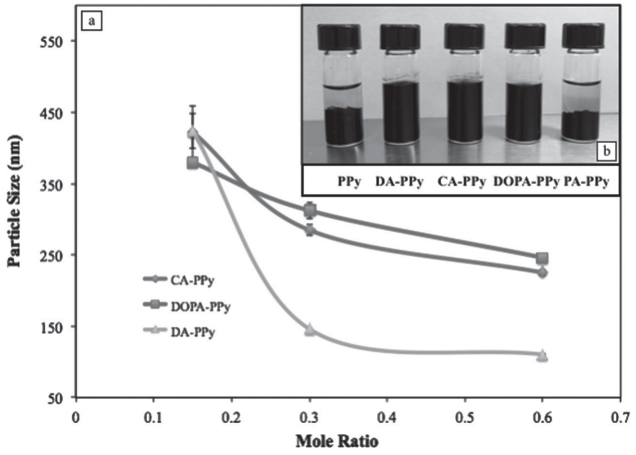

Figure 5. a) Plots of hydrodynamic radius verses catechol/Py mole ratio of DLS experiment; and b) digital photo of vials with 3 mL water-dispersed pure and modified PPy suspension after 5 h.

DLS analyses were performed to investigate the changes of hydrodynamic diameter with respect to the catechol/Py mole ratio. Note that catechol-PPy synthesized with low catechol/Py mole ratios from 0 to 0.064, PA-PPy, and pristine PPy cannot be measured by the DLS due to the rapid aggregation of particles. **Figure 5**a showed that the hydrodynamic diameter of DA-PPy decreased from 430 to 110 nm, CA-PPy decreased from 420 to 220 nm, and DOPA-PPy decreased from 380 to 250 nm when the catechol/Py reacting mole ratio increased from 0.16 to 0.64. The smaller hydrodynamic diameter at higher catechol/Py mole ratio may contribute to the better dispersion of functionalized PPy. To examine the dispersion property of modified PPy, the pristine PPy, DA-PPy, CA-PPy, DOPA-PPy, and PA-PPy composites were dispersed in water separately. After ultrasonicated for 5 min, the samples were allowed to rest at room temperature. Figure 5b presented digital photos of the dispersion of each sample in deionized (DI) water after 5 h, it was found that pure PPy and PA-PPy destabilized and precipitated immediately. By contrast, catechol derivative modified PPy exhibited excellent water dispersibility due to the presence of hydrophilic catechol groups. Moreover, for DA-PPy, CA-PPy, and DOPA-PPy composites, a higher catechol/Py mole ratio also led to better dispersion. The improved water dispersibility of the catechol-modified PPy composite is beneficial for its applications in practical engineering.

To further analyze the PPy system, we performed XPS measurements on pure PPy and (DA, CA, DOPA, and PA)-PPy at different ratios to characterize the surface composition. As shown in Table S1 (Supporting Information), the corresponding content of oxygen of DA-PPy increased from 22.3% to 28.4%, CA-PPy increased from 19.9% to 23.6%, and DOPA-PPy increased from 19.1% to 21.9%, when the catechol/Py reacting mole ratio increased from 0.032 to 0.64. Due to the fact that there is no oxygen species in pristine PPy, the oxygen content increase may be explained by the effect that catechols were successfully grafted onto the PPy surface, likely through both covalent bonds and the noncovalent forces (charge transfer, π-stacking, and hydrogen bonding interactions). Furthermore, compared with pure PPy, the value of N/C ratio increased for all three catechol derivatives-modified PPy at 0.64 catechol/Py reacting mole ratio, which is consistent with the theoretical values that catechols have higher N/C ratio than PPy. The above results further confirmed the presence of catechols on the modified PPy surface. For PA-modified PPy at both low and high PA concentration, there is no significant change on the surface composition compared with pure PPy, indicating PA had a negligible influence on PPy structure. It is noted that the pure PPy surface showed the presence of oxygen (530 eV, O 1 s) and sulfur (170 eV, S 2p), which might be introduced from the oxidizing agent ammonium persulfate.

2.2. Adhesion Properties of Functionalized PPy

Our previous research findings indicated that the adhesion strength between DA-PPy film and glass substrate were significantly improved by combining mussel-adhesive inspired molecule DA into the synthesis of PPy nanofibers. In this work, we investigated the adhesion properties of DA, CA, DOPA, and PA-modified PPy film, respectively aiming to determine which functional component is critical for achieving strong adhesion. The adhesion properties of modified PPy were characterized by a 180° peeling test, which is applied to examine the bonding strength between the modified PPy film and glass substrate. We have adopted the tape/PPy/glass system, where the failure may occur either at the tape/PPy or PPy/glass interface. Two examples were presented in **Figure 6**a, which are the typical force versus displacement curves of peeling PPy nanofiber films from glass substrate at 0.032 and 0.64 DA/Py mole ratio at 15 mm s^{-1} peeling speed. Curve 1 shows the case of an interfacial failure between the glass slide and PPy film, i.e., the delamination of PPy film from glass; curve 2 shows the case of a failure at tape/PPy film interface at a higher DA/Py mole ratio. Four peeling parameters, illustrated in Figure 6a, can be extracted from curve 1: peak peel force (F_p), steady-state force (F_{ss}), initiation distance (D_i), and transition distance (D_t).[30] In our system, the peak force (F_p) (i.e., the force required to initiate failure) has been utilized to compare the adhesion between glass and modified PPy films.

Figure 6b plotted the peak force versus catechol/Py mole ratio of four modified PPy films at constant peeling rate 15 mm s^{-1}. For catechol derivatives' functionalized PPy films, we observed a clear trend that F_p increased with the catechol mole percentage. Moreover, the interfacial failure shifted from film/glass to tape/film interfaces with increased catechol/Py mole ratio, indicating strong bonding between catechol-PPy and glass. It is also important to note that adding only a small amount of catechol derivatives can dramatically improve the PPy adhesion, which is about three orders of magnitude higher than that of pure PPy. On the contrary, PA modification had almost negligible influence on the PPy adhesion property, and PA-PPy film self-delaminated from the glass was observed at all PA/Py mole ratios. It is concluded that instead of amine functional group or coexistence of both catechol and amine moieties, catechol functional group itself is responsible for the adhesion improvement of PPy film. Such discovery is consistent with literature data. Deming and co-workers performed tensile shear strength measurements on a catechol-containing polypeptide to evaluate its adhesion property;[31] they also found that the adhesive strength of this

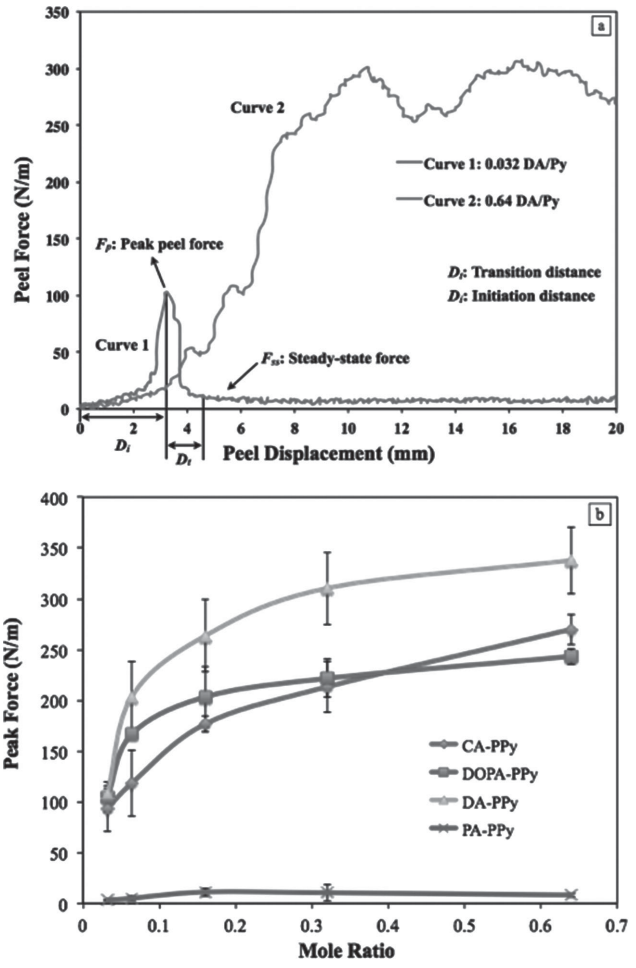

Figure 6. a) Peeling curves of 0.032 and 0.64 DA/Py mole ratio PPy film with 15 mm s^{-1} peeling speed, and the illustration of four peeling parameter: peak peel force (F_p), steady-state force (F_{ss}), initiation distance (D_i), and transition distance (D_t). b) Plots of the peak force verses (DA, CA, DOPA, and PA) /Py mole ratio at a constant peeling speed rate of 15 mm s^{-1}.

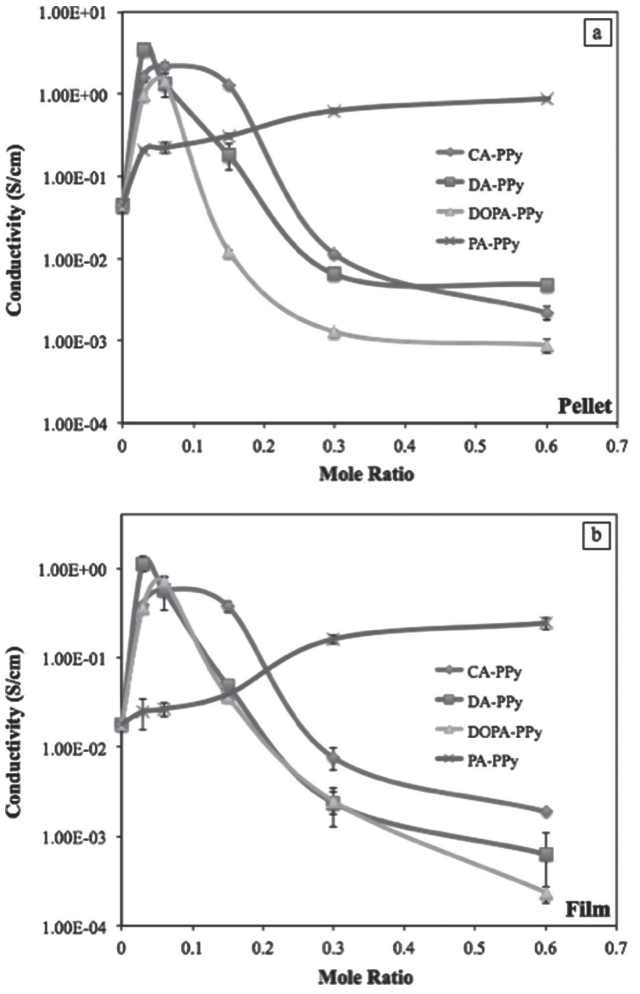

Figure 7. Electrical conductivity of the DA, CA, DOPA, and PA-modified PPy compressed pellets; a) and the casted film b) with various (DA, CA, DOPA, and PA)/Py mole ratios.

co-polymer was proportional to the amount of catechol moieties in the polymer backbone, but independent of the choice of oxidizing agents. Smaller particle size is another factor that may contribute to the strong catechol-PPy adhesion. Smaller sized particles provide lager surface area, whereas more interactions (hydrogen bonding and van der Waals forces) can be formed at the film/glass interface. Moreover, it was noticed that solution with a smaller particle size yielded smoother and more uniform films with less roughness. As a result, the effective contact area between the modified PPy film and the tape would increase with the catechol/Py mole ratio, responsible for the increased adhesion force F_p as shown in Figure 6b.

2.3. Electrical Properties of Functionalized PPy

To investigate how different functional groups affect PPy material properties, the electrical conductivity of catechols and PA-modified PPy with various (DA, CA, DOPA, PA)/Py mole ratios were measured by a standard four-point probe setup. Owing to the fact that porosity, density, and packing structure may affect the overall conductivity of PPy nanofibers, both powder compressed pellet and solution-casted film were prepared and their conductivities are shown in **Figure 7**. The electrical conductivity of pristine PPy is about 0.04 S cm^{-1} for pellet and 0.01 S cm^{-1} for film. For all three catechol derivatives, as the catechol/Py mole ratio is increased, the electrical conductivity increased and reached a maximum value of 3.8 S cm^{-1} for DA-PPy pellet, 1.1 S cm^{-1} for DA-PPy film, 2.2 S cm^{-1} for CA-PPy pellet, 0.6 S cm^{-1} for CA-PPy film, 1.4 S cm^{-1} for DOPA-PPy pellet, and 0.7 S cm^{-1} for DOPA-PPy film. We attributed the conductivity improvement to the following reasons: (1) PPy morphology shifted from globular into fibrous after catechol modification, and fiber structure is more effective for charge transport; (2) catechol derivatives are acidic in water, therefore they may act as a dopant to provide more positive charges on the polymer backbone for the electrical conduction; (3) the intrinsic adhesion properties of catechol moieties brought PPy fibers closer and denser packed, thus increased the contact area among individual fibers and stronger conductive network was formed for better electron movement. However,

the conductivities of both PPy compressed pellets and films decreased as the catechol/Py mole ratio increased from 0.064 to 0.64. It can be explained by the fact that catechol functional groups may selfadhere to the PPy surface via covalent bonding, π–π stacking and hydrogen bonding, and the degree of coverage increased with the catechol derivative concentration. As a result, the insulating catechol moieties may block the electron transfer among each PPy polymer chain at high catechol/Py mole ratio. Moreover, after incorporating catechol derivatives into the PPy chain, especially at high catechol concentration, the PPy chain length was significantly reduced, which may decrease the effective conjugation length and minimize the efficiency of charge hopping to lower the overall conductivity. For PA-modified PPy, there is no chemical reaction between PA and Py since the morphology and particle size remain the same as pristine PPy; however, the conductivity of PA-PPy composite and film increased when the content of PA is increased as shown in Figure 7. This might be because PA is in a form of 2-phenylethylamine hydrochloride salt, where hydrochloride can dope the system to increase PPy conductivity. Noted that DA is also in a form of dopamine hydrochloride salt, but compared with PA-PPy system, acid doping is not the only factor that may affect the DA-PPy conductivity, other reasons including morphology change and DA adhesion property should also be considered to explain the overall DA-PPy conductivity change as discussed above.

Figure 8 shows the UV–vis absorption spectra of the modified PPy at different catechol/Py molar ratios. Note that PA-PPy and pristine PPy cannot be measured by UV–vis spectroscopy due to poor water dispersion. All spectra displayed two distinct peaks at around 350 and 700 nm. The first absorption band is associated with the π–π^* transition from valence band to the polaron/bipolaron bands, while the second feature is due to the conduction electrons at the bipolaron state of PPy. For DA-modified PPy, a significant blue-shift of the π–π^* transition peak from 450 to 351 nm was observed with increasing DA/Py mole ratio. The blue shift of π–π^* transition absorption suggests that the conjugation degree of DA-modified PPy was decreasing. For CA and DOPA-modified PPy, we found a slight red-shift of the peak with increasing CA/Py and DOPA/Py mole ratio from 0.032 to 0.064. However, when the CA/Py and DOPA/Py mole ratio increased from 0.064 to 0.64, there was a blue-shift of the peak from 359 to 351 nm for CA-PPy and from 377 to 349 nm for DOPA-PPy. These observations agreed with our four-probe measurement that the conductivity of DA-PPy decreased with increasing DA/Py ratio from 0.032 to 0.64, while the conductivity of CA-PPy and DA-PPy increased to a maximum value and then decreased with increasing CA/Py and DA/Py mole ratio. It is noted that Wu et al. also reported the blue shift of UV–vis spectra on PPy-cellulose nanocrystal (CNC) system with increasing Py/CNC mole ratio, they attributed the blue shift to the disorder and defects introduced to the polymeric chains, resulting in the decrease of overall conductivity.[32]

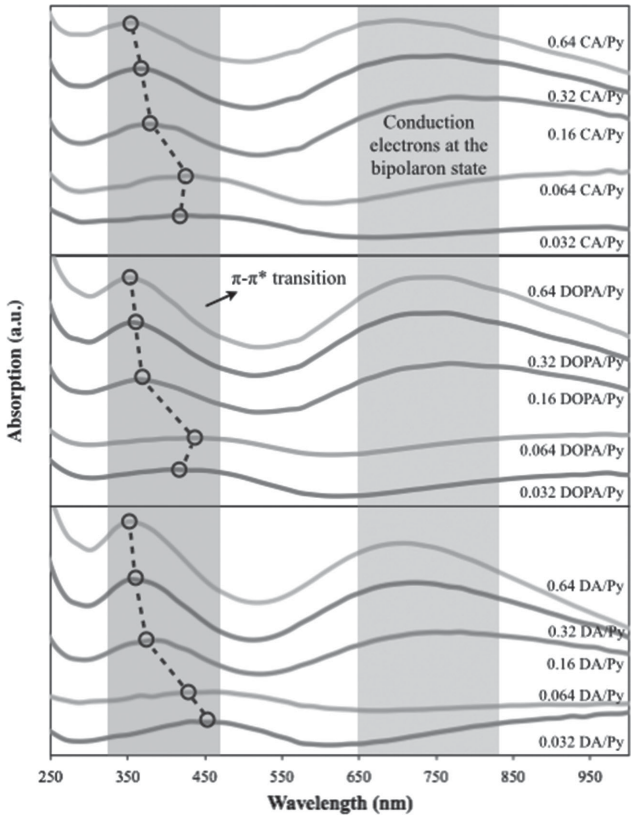

Figure 8. UV–vis spectra of catechol-PPy synthesized with various catechols/Py ratios. The π–π^* transition peaks were obtained at local maxima and indicated in black circles.

To further investigate the electrical properties of catechol modified PPy, their bandgap energies (E_g) were calculated from the UV–vis spectra by the Tauc plot, which is described as[33]

$$(\alpha h\nu)^n = C \times (h\nu - E_g)$$

where α is the absorption coefficient, h is Planck's constant, ν is the frequency of light, C is the proportionality constant, and n is the exponent denoting the optical transition process. The values of n can be 1/2, 3/2, 2, and 3, indicating direct allowed, direct forbidden, indirect allowed, and indirect forbidden transitions, respectively.[34] The absorption coefficient is defined by the following equation deduced from Beer–Lambert's relation[35]

$$\alpha = -\frac{1}{t} \times \ln\left(\frac{I_t}{I_0}\right) = \frac{1}{t} \times A \times \log_{10} e$$

where A, t, I_t, and I_0 represent the absorbance determined from the UV–vis spectrum, path length of the quartz cuvette, intensity of transmitted light, and intensity of incident light, respectively. The bandgap E_g can be estimated by extrapolating the straight part of $(\alpha h\nu)^n$ versus $h\nu$ curve to the $h\nu$ axis by linear fitting.[34–37] **Figure 9**a–c plotted $(\alpha h\nu)^2$ as a function of photon energy $(h\nu)$, where $n = 2$ since the optical transitions for amorphous semiconductors are described as indirect allowed transitions; the linear extrapolated lines are shown as black dash lines. From Tauc plots, the optical bandgaps of DA-PPy, CA-PPy, and DOPA-PPy at varied catechol/Py reacting mole ratios were summarized in Figure 9d. It was estimated that the bandgap E_g increased from 3.46 to 4.94 eV for DA-PPy; this increase in E_g indicated that more energy needed to promote an electron from valence to the conduction band, and as a result, electronic conductivity dropped with increasing DA/Py mole ratio. For CA-PPy and DOPA-PPy system, the E_g value dropped first and

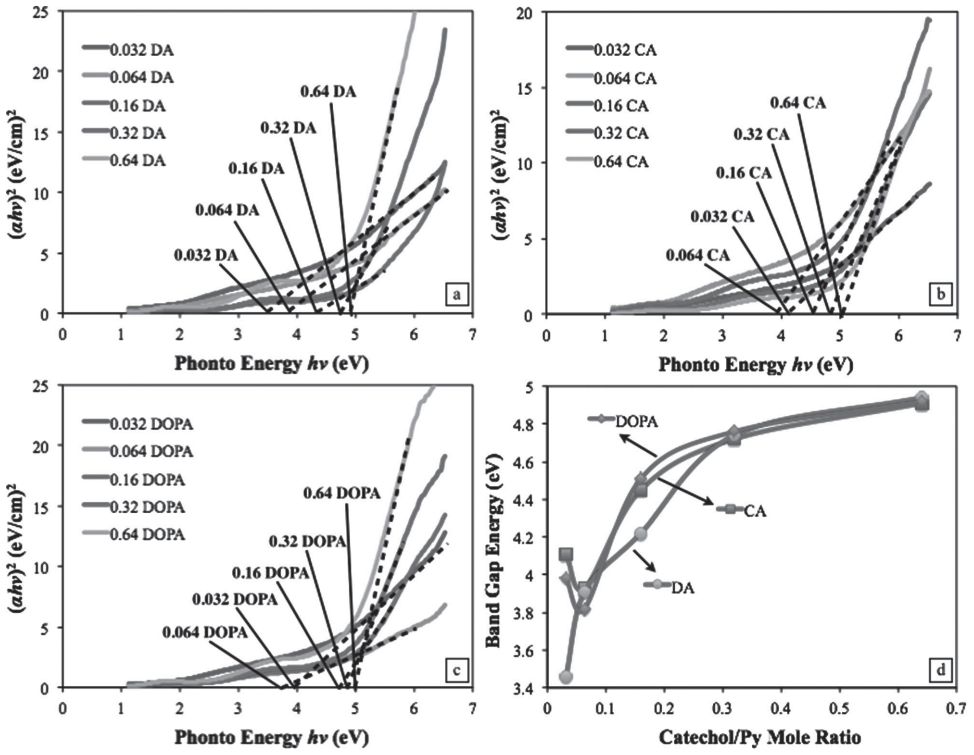

Figure 9. Plots of optical bandgap of the a) DA-PPy; b) CA-PPy; and c) DOPA-PPy. d) Plot of the bandgap energy of DA-PPy, CA-PPy, and DOPA-PPy with various catechol/Py ratios.

then became larger with increasing CA/Py and DOPA/Py mole ratio, which agreed with the conductivity results of Figure 7.

2.4. Scratch Resistances of DA-PPy and its PVA Nanocomposite Coating Films

Both improved adhesion and conductivity make catechol functionalized PPy a promising candidate for thin film coating in microelectrical applications, where the durability, mechanical behavior of the coating film is almost equally important as the function of the thin film itself. As a result, we employed ASTM standard scratch test to produce and evaluate PPy film surface damage under controlled stress or load.[38] The tests were performed on a DA-functionalized PPy film resulting from 0.064 DA/Py mole; we choose this sample among the three catechols functionalized PPy because DA-PPy exhibited the smallest particle size and the best performance in both adhesion and electrical conductivity. **Figure 10**a presented a typical scratch track of induced damages on DA-PPy film along with the increasing load under an optical microscope. The critical load—the maximum load that a DA-PPy film can withstand prior to delamination—was obtained to determine the conditions in which, the PPy coating can be safely used. As shown in the image, film delamination began almost immediately after scratch started at about 76 g, suggesting a relatively poor scratch resistance of DA-PPy film.

In order to enhance the mechanical properties of the PPy film for its effective transfer into practical engineering, we dispersed DA-PPy nanofibers into PVA, which is an excellent polymer binder due to its high water solubility, good adhesion, and biocompatibility. Thanks to the catechol modification, the hydroxyl groups in PVA could strongly interact with DA-PPy, forming uniform dispersion that was readily casted into thin films. Two DA-PPy/PVA polymer films were prepared by casting the as-synthesized DA-PPy dispersed in 1 and 2 wt% PVA aqueous solution. Figure 10b exhibited optical images of the scratch trace on DA-PPy film prepared with 1 wt% PVA solution deposited on glass substrate. There was a small amount of deformation, including fully recoverable elastic, time-dependent viscoelastic and nonrecoverable plastic deformation, observed under low load level (0–420 g). During the period of the normal load of the tip linearly ramped from the minimum to the maximum during sliding, the film damages transferred into plowing 420–323 g (Figure 10c) and stick-slip behavior 1323–1655 g (Figure 10d), followed by snag point 2037 g (Figure 10e) and film delamination 2901 g (Figure 10f). The critical load and conductivity for the films casted from DA-PPy dispersed in pure water and DA-PPy dispersed in 1 wt% PVA and 2 wt% PVA aqueous solutions were compared at Figure 10g. It is clear that PVA matrix significantly improved the DA-PPy film scratch resistance and maintained high mechanical integrity. Noted that the film thickness of three samples were measured to be almost identical, thus the film thickness difference have negligible effect on the scratch test results. The electrical conductivity of DA-PPy film and DA-PPy film prepared with 1 wt% PVA solution were measured to be 0.056 S cm^{-1} and 0.039 S cm^{-1}, but for DA-PPy film prepared with 2 wt% PVA solution, the conductivity dropped to 1.6×10^{-5} S cm^{-1}. It is also informative to note that films casted by unmodified PPy

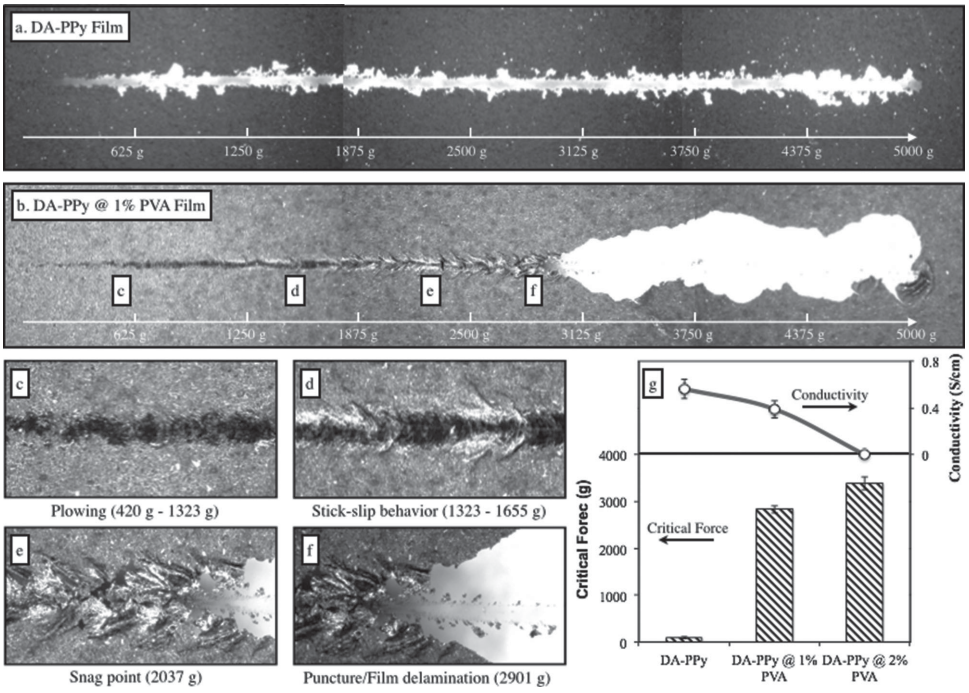

Figure 10. Damages observed on test film surface using the scratch test: a) DA-PPy film; b) DA-PPy film prepared with 1 wt% PVA solution. Different failures observed on DA-PPy film prepared with 1 wt% PVA solution: c) plowing; d) stick-slip behavior; e) snag point; and f) film delamination. g) Plot of critical load and conductivity for pure DA-PPy film and DA-PPy film prepared with 1 wt% PVA and DA-PPy film prepared with 2 wt% PVA solutions.

prepared with 1 wt% PVA solution showed nonuniform dispersibility and almost insulating behavior.

Finally, it would be useful to discuss the technical implications of the DA-PPy added with PVA for its practical applications. Recently, Hu et al. reported that polydopmaine (PDA) itself could be used as a filler to improve the thermal, mechanical, and adhesive performance of PVA polymer.[39] Our DA-PPy nanofibers could be used to replace the PDA as so to introduce an additional function—high electrical conductivity to this composite, further widening its potential applications, such as electrical conductive adhesives (ECAs). Traditional ECAs are based on silver-filled polymer composites, which are relatively expensive and nonenvironment friendly.[40] Their preparation processes also require the use of a solvent, curing agent, or stabilizer, thus their applications in biotechnology are limited. To achieve better biocompatibility, another conducting polymer polyaniline (PANI)-based PVA composite was prepared, but it suffers from poor conductivity (4.3×10^{-6} S cm^{-1}).[41] In this respect, biocompatible DA-PPy/PVA materials with moderate conductivity (0.039 S cm^{-1}), could replace traditional ECAs to be used in many biological-relevant applications, including artificial muscles, scaffold, and biosensors.

3. Conclusions

In summary, we reported a benign one-step approach to synthesize novel catechol-PPy nanofibers. After comparing the morphology, particle size, dispersibility, adhesion, and electrical conductivity of the PPy modified by dopamine hydrochloride (DA), 1,2-dihydroxybenzene (CA), DOPA, and phenylethylamine (PA), respectively, we demonstrated that dicatechol functional group is responsible for most of the PPy property changes. The catechol moieties can be oxidized into *o*-quinonimine, which can chemically react with Py ring to regulate the polymer chain growth, forming unique fibrous PPy structure and smaller PPy particle size. The catechol-PPy also inherited the intrinsic adhesion properties of catechols, and the bonding strength between catechol-PPy and glass substrate was significantly enhanced. Due to the strong adhesion and acidic nature of catechol, the electrical conductivity of modified PPy was also improved at low catechol/Py mole ratios. Moreover, we found that modified PPy can be uniformly dispersed into PVA polymer matrix and casted to form thin film coating via a convenient solution-cast method, as-prepared coating exhibited high scratch resistance, biocompatibility and conductivity, will find broad industrial applications. In addition, this work could open new opportunities of using catechol derivatives to functionalize more conductive polymers for better mechanical and electrical performance.

4. Experimental Section

Materials: Pyrrole (Py, 98%), ammonium persulfate (APS), DA, 1,2-dihydroxybenzene (CA), DOPA, 2-phenylethylamine hydrochloride (PA), and polyvinyl alcohol (PVA) were purchased from Sigma-Aldrich and used as received. Modified DA-PPy was prepared by the following procedures. In a typical experiment, 0.12 mL or 0.116 g pyrrole monomer and certain amount of dopamine hydrochloride (0.01, 0.02, 0.05, 0.1, and 0.2 g) were dissolved in 25 mL tris solution (pH = 8.5, 10×10^{-3} M) and cooled down to 8 °C on a cooling plate. APS/tris solution (0.5 g/5 mL) was added to the DA/Py solution dropwisely under vigorous stirring for

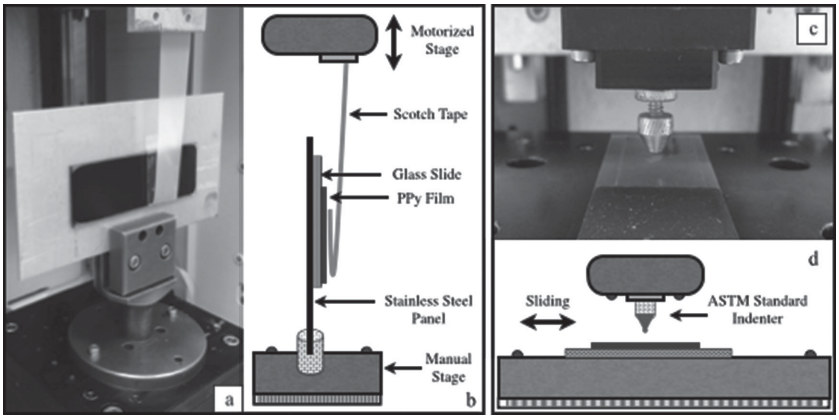

Figure 11. a) Digital photo of a typical peeling test set up; b) A schematic illustration of the 180° peeling test; c) digital photo of a typical scratch test set up; and d) a schematic illustration of the scratch test.

18 h at a reaction temperature maintained at 8 °C. The precipitates were filtered and collected by centrifuging resulted solution and sequentially washing with deionized water for 5 times. The washed precipitates were then freeze-dried for 24 h to produce powder materials. The above procedures were also applied to prepare CA-PPy, DOPA-PPy, and PA-PPy nanofibers at different mole ratios.

Film Fabrication: Modified PPy films were prepared by solution casting method. In a typical experiment, 1 mL of DA-PPy solution was directly cast into film on a 2 × 4 cm glass slide and dried at 80 °C for 5 h, and the samples were tested within 30 min after taking out from the oven to avoid moisture accumulation on the film. For fabricating DA-PPy/PVA films, 20 wt% DA-PPy dry powders were dispersed in 1 wt% PVA and 2 wt% PVA aqueous solution, respectively, then 1 mL as-prepared solution was directly casted into film on a 2 × 4 cm glass slide and dried at 80 °C for 5 h. The film's thickness of DA-PPy, DA-PPy prepared with 1% PVA and DA-PPy with 2% PVA solutions were measured to be 30 ± 2 μm by an optical profiler (MFP-D WLI 3D surface profilometer, Rtec Instruments Inc, USA).

Methods: For high resolution transmission electron microscope (HRTEM, JEOL 2010F FEG) and scanning electron microscope (SEM, Zeiss LEO 1550) experiments, the washed PDA-PPy dry powders were used. In the dynamic light scattering (DLS, Malvern Zetasize nano series Nano ZS90) and UV–vis spectroscopy (Agilent 8453A) experiments, freeze dried powder was redispersed in water and measured as quickly as possible to avoid particle aggregation, and on an average, each spectrum was completely recorded within 3 min. X-ray photoelectron spectroscopy (XPS, monochromatic Al Ka X-ray source, Thermo Scientific Alpha) was used to analyze the surface atomic composition of the modified PPy samples. The electrical resistivity of PPy composites and films were measured by a four-point probe setup that consists of a probe fixture (Cascade microtech Inc.) and a source meter (Keithley 2440 5A Source Meter, Keithley Instruments Inc.). The resistivity was calculated by using a standard method in literature[42]

$$\rho = F\frac{\pi t}{\ln 2}\times\frac{V}{I}(\Omega\text{cm})$$

where t, I, V, and F represent the pellet/film thickness, applied current, read-out voltage, and dimensionless correction factor, respectively. The value of F depends on the ratio of t/s, where s is the probe spacing (s = 0.1 mm). From the four-point probe theory, F equals to 1 as t/s approaches 0. In our system, t/s equal to 0.1 for pellet and 0.015 for film, so we approximate F = 1. Peeling tests were performed on the same Universal Materials Tester (UMR-1, CERT) shown in **Figure 11**a. A schematic illustration of the 180° peeling is presented in Figure 11b. In a typical experiment, a glass substrate was fixed onto a stainless steel panel with double-sided tape. The backing Scotch tape was placed onto the PPy film with about 200 g pressing force to remove the air bubbles between the tap and the film. The top of the tape was gently folded back at 180°; the tapes were then peeled from the bottom toward top of the film at a speed of 5 or 15 mm s^{-1}. The displacement, peeling forces, and time were recorded by a commercial UMT program for further analysis. Scratch tests were performed on the same Universal Materials Tester (UMR-1, CERT) shown in Figure 11c. A schematic illustration of the scratch tests is presented in Figure 11d. The scratch indenter was an ASTM standard 1 mm diameter stainless steel ball, which was mounted to a 10 kg load cell. In a typical experiment, the indenter was brought into contact with a substrate at a speed rate of 5 μm s^{-1} until a normal force of 1 g was reached. Then, the indenter was moved 20 mm horizontally along the film surface at a sliding speed of 0.1 mm s^{-1} while keeping the normal force linearly increased at 25 g s^{-1} to a maximum of 5 kg. The scratch track was then examined under a digital microscope (AD4113ZT, Dino-Lite) and analyzed by ASTM standard methods (D7027-test mode A).[43]

Supporting Information

Supporting Information is available from the Wiley Online Library or from the author.

Acknowledgements

The authors would like to thank the Natural Sciences and Engineering Research Council of Canada (NSERC) and the Ministry of Research and Innovation of Ontario for the financial support.

Received: September 9, 2014
Revised: January 8, 2015
Published online: January 29, 2015

[1] Q. Ye, F. Zhou, W. Liu, *Chem. Soc. Rev.* **2011**, *40*, 4244.
[2] R. A. Wise, *Nat. Rev. Neurosci.* **2004**, *5*, 483.
[3] J. H. Waite, *Annu. Rev. Mater. Res.* **2011**, *41*, 99.
[4] J. Saiz-Poseu, J. Sedo, B. Garcia, C. Benaiges, T. Parella, R. Alibes, J. Hernando, F. Busque, D. Ruiz-Molina, *Adv. Mater.* **2013**, *25*, |2066.
[5] E. Faure, C. Falentin-Daudré, C. Jérôme, J. Lyskawa, D. Fournier, P. Woisel, C. Detrembleur, *Prog. Polym. Sci.* **2013**, *38*, 236.
[6] H. Lee, N. F. Scherer, P. B. Messersmith, *Proc. Natl. Acad. Sci. U.S.A.* **2006**, *103*, 12999.
[7] J. Sedó, J. Saiz-Poseu, F. Busqué, D. Ruiz-Molina, *Adv. Mater.* **2013**, *25*, 653.
[8] D. Kaneko, K. Matsumoto, S. Kinugawa, S. Tateyama, T. Kaneko, *Polym. J.* **2011**, *43*, 944.
[9] S. Moulay, *Polym. Rev.* **2014**, *54*, 436.
[10] B. P. Lee, J. L. Dalsin, P. B. Messersmith, *Biomacromolecules* **2002**, *3*, 1038.
[11] G. Westwood, T. N. Horton, J. J. Wilker, *Macromolecules* **2007**, *40*, 3960.
[12] E. Karabulut, T. Pettersson, M. Ankerfors, L. Wågberg, *ACS Nano* **2012**, *6*, 4731.
[13] Y. Liu, K. Ai, L. Lu, *Chem. Rev.* **2014**. *114*, 5057.
[14] H. Lee, S. M. Dellatore, W. M. Miller, P. B. Messersmith, *Science* **2007**, *318*, 426.

[15] D. R. Dreyer, D. J. Miller, B. D. Freeman, D. R. Paul, C. W. Bielawski, *Chem. Sci.* **2013**, *4*, 3796.
[16] J. Yan, L. Yang, M. F. Lin, J. Ma, X. Lu, P. S. Lee, *Small* **2013**, *9*, 596.
[17] Y. Zhang, B. M. Teo, A. Postma, F. Ercole, R. Ogaki, M. Zhu, B. Stadler, *J. Phys. Chem. B* **2013**, *117*, 10504.
[18] W. Zhang, F. K. Yang, Y. Han, R. Gaikwad, Z. Leonenko, B. Zhao, *Biomacromolecules* **2013**, *14*, 394.
[19] F. K. Yang, W. Zhang, Y. Han, S. Yoffe, Y. Cho, B. Zhao, *Langmuir* **2012**, *28*, 9562.
[20] W. Zhang, F. K. Yang, Z. Pan, J. Zhang, B. Zhao, *Macromol. Rapid Commun.* **2014**, *35*, 350.
[21] N. Gomez, J. Y. Lee, J. D. Nickels, C. E. Schmidt, *Adv. Funct. Mater.* **2007**, *17*, 1645.
[22] M. Pyo, C. C. Bohn, E. Smela, J. R. Reynolds, A. B. Brennan, *Chem. Mater.* **2003**, *15*, 916.
[23] F. Faverolle, A. J. Attias, B. Bloch, P. Audebert, C. P. Andrieux, *Chem. Mater.* **1998**, *10*, 740.
[24] Y. Z. Long, M. M. Li, C. Gu, M. Wan, J. L. Duvail, Z. Liu, Z. Fan, *Prog. Polym. Sci.* **2011**, *36*, 1415.
[25] S. De Vito, C. R. Martin, *Chem. Mater.* **1998**, *10*, 1738.
[26] X. Zhang, S. K. Manohar, *J. Am. Chem. Soc.* **2005**, *127*, 14156.
[27] J. Zhang, X. Liu, L. Zhang, B. Cao, S. Wu, *Macromol. Rapid Commun.* **2013**, *34*, 528.
[28] J. Joo, J. K. Lee, J. S. Baeck, K. H. Kim, E. J. Oh, J. Epstein, *Synth. Met.* **2001**, *117*, 45.
[29] P. Pfluger, G. B. Street, *J. Chem. Phys.* **1984**, *80*, 544.
[30] B. Zhao, R. Pelton, *J. Adhes. Sci. Technol.* **2003**, *17*, 815.
[31] M. Yu, T. J. Deming, *Macromolecules* **1998**, *31*, 4739.
[32] X. Wu, V. L. Chabot, B. K. Kim, A. Yu, R. M. Berry, K. C. Tam, *Electrochim. Acta* **2014**, *138*, 139.
[33] J. Tauc, *Mater. Res. Bull.* **1968**, *3*, 37.
[34] D. B. Buchholz, J. Liu, T. J. Marks, M. Zhang, R. P. Chang, *ACS Appl. Mater. Interfaces* **2009**, *1*, 2147.
[35] Z. Khan, M. Khannam, N. Vinothkumar, M. De, M. Qureshi, *J. Mater. Chem.* **2012**, *22*, 12090.
[36] J. Hazarika, A. Kumar, *Nucl. Instrum. Methods Phys. Res., Sect. B* **2014**, *318*, 269.
[37] H. Gherras, A. Hachemaoui, A. Yahiaoui, A. Benyoucef, A. Belfedal, M. Belbachir, *Synth. Met.* **2012**, *162*, 1750.
[38] O. Borrero-López, M. Hoffman, A. Bendavid, P. J. Martin, *Thin Solid Films.* **2010**, *518*, 4911.
[39] S. Xiong, Y. Wang, J. Yu, L. Chen, J. Zhu, Z. Hu, *J. Mater. Chem. A.* **2014**, *2*, 7578.
[40] B. M. Amoli, S. Gumfekar, A. Hu, Y. N. Zhou, B. Zhao, *J. Mater Chem.* **2012**, *22*, 20048.
[41] S. P. Gumfekar, W. Wang, B. Zhao, *Macromol. Mater. Eng.* **2014**, *299*, 966.
[42] N. W. Pu, Y. Y. Peng, P. C. Wang, C. Y. Chen, J. N. Shi, Y. M. Liu, M. D. Ger, C. L. Chang, *Carbon* **2014**, *67*, 449.
[43] ASTM D-7027, "Standard Test Method for Evaluation of Scratch Resistance of Polymeric Coatings and Plastics Using an Instrumented Scratch Machine", ASTM International.